How to cite:
International Edition: doi.org/10.1002/anie.202109027
German Edition: doi.org/10.1002/ange.202109027

CO_2 Hydrogenation

Moderate Surface Segregation Promotes Selective Ethanol Production in CO_2 Hydrogenation Reaction over CoCu Catalysts

Sihang Liu, Chengsheng Yang, Shenjun Zha, Dmitry Sharapa, Felix Studt, Zhi-Jian Zhao, and Jinlong Gong*

Abstract: *■■1) Headline ok? 2) Are all acronyms defined when first mentioned and applied thereafter?■■Cobalt-copper (CoCu) catalysts have industrial potential in CO/CO_2 hydrogenation reactions, and CoCu alloy has been elucidated as a major active phase during reactions. However, due to elemental surface segregation and dealloying phenomena, the actual surface morphology of CoCu alloy is still unclear. Combining theory and experiment, the dual effect of surface segregation and varied CO coverage over CoCu(111) surface on the reactivity in CO_2 hydrogenation reactions is explored. The relationship between C−O bond scission and further hydrogenation of intermediate *CH_2O was discovered to be a key step to promote ethanol production. The theoretical investigation suggests that moderate Co segregation provides a suitable surface Co ensemble with lateral interactions of co-adsorbed *CO, leading to promoted selectivity to ethanol, in agreement with theory-inspired experiments.*

Introduction

In the past decade, CoCu bimetallic catalysts have shown potential industrial applications in CO/CO_2 hydrogenation processes.[1] Distinct from traditional Cu/ZnO/Al_2O_3 catalysts for CO_2 hydrogenation,[2] CoCu alloys show promising reactivity for the production of ethanol and other higher alcohols, possibly due to the bifunctionality introduced by the presence of cobalt and copper during hydrogenation reactions.[3] It is indicative that by changing the surface composition of CoCu alloys, the reactivity and selectivity in hydrogenation reactions could be modified, an appropriate Co-Cu elemental distribution has been suggested crucial to produce higher alcohols with a high selectivity.[3b] Though several theories have been proposed to explain the high selectivity towards higher alcohols over CoCu bimetallic alloys, the atomic structure-performance relationship remains elusive, due to the mechanistic complexity of higher alcohol production.[4]

An in-depth analysis of the CoCu surface composition is complicated by the fact that CoCu alloys are prone to surface segregation, a result of the large difference in surface energies and binding strength to adsorbates. Consequently, core–shell CoCu structures and even de-alloyed phases have been frequently observed in previous experiments,[5] and also been predicted by theory.[6] As expected from their physical properties, Cu tends to segregate to the surface in vacuum or in an atmosphere with relatively inert gases, while the inverse surface segregation of Co takes place when exposed to Co-preferred adsorbates such as carbon monoxide.[7] Therefore, coverage effects and lateral interactions of co-adsorbates also play a role in CoCu-catalyzed reactions, as they dictate changes in the adsorption strength of reaction intermediates and corresponding reaction barriers, thus greatly influencing the selectivity. This entanglement of surface segregation and induced coverage effect makes it a big challenge to study the catalytic nature of active sites over CoCu surfaces and similar alloy systems.[8]

Herein, combining DFT-based surface phase diagram and a prereduction-controlled surface segregation method, we unveil the actual surface composition of CoCu alloys as a function of CO pressures and address the dual roles of surface segregation and induced coverage effects. A moderate Co-segregated surface was identified as a crucial promotor to ethanol production, while low Co-segregated surfaces were responsible for catalyzing CO_2 hydrogenation to methanol and high Co-segregated surfaces suffer from severe self-poisoning. We believe that the insight in this work provides a new paradigm for theory-based catalyst optimization.

In previous work, we found that split H_2 adsorbed on the surface has no ability to drive Co segregation under temperatures usually applied in CO_2 hydrogenation reactions, while

[*] S. Liu, Dr. C. Yang, Prof. Dr. Z. Zhao, Prof. Dr. J. Gong
Key Laboratory for Green Chemical Technology of Ministry of Education, School of Chemical Engineering and Technology, Collaborative Innovation Center of Chemical Science & Engineering, Tianjin University
Weijin Road 92, Tianjin, 300072 (China)
E-mail: ■■email missing■■
Prof. Dr. J. Gong
Joint School of National University of Singapore and Tianjin University, International Campus of Tianjin University
Binhai New City, Fuzhou 350207 (China)
S. Zha, Dr. D. Sharapa, Prof. Dr. F. Studt
Institute of Catalysis Research and Technology, Karlsruhe Institute of Technology
Hermann-von-Helmholtz-Platz 1, 76344 Eggenstein-Leopoldshafen (Germany)
and
Institute for Chemical Technology and Polymer Chemistry, Karlsruhe Institute of Technology
Engesserstr. 18, 76131 Karlsruhe (Germany)
S. Liu
Present address: Catalysis Theory Center, Department of Physics, Technical University of Denmark (DTU)
2800 Kgs. Lyngby (Denmark)
Supporting information and the ORCID identification number(s) for the author(s) of this article can be found under: https://doi.org/10.1002/anie.202109027.

adsorbed *CO induces segregation of Co.[9] To model the CoCu alloy, we chose a 5-layer 3×3 CoCu(111) surface as the catalyst model, which is large enough to describe surface segregation tendencies under different CO pressures and can also be subsequently used to calculate the hydrogenation reactions in detail. The temperatures set in this work are 473 K and 723 K, corresponding to the reaction temperature applied in CO_2 hydrogenation reactions and CO pre-reduction temperature, respectively. To enhance the surface screening procedure, we applied a revised genetic algorithm[10] to globally optimize *n*CO-(3×3)-CoCu(111) surfaces, with n ranges from 0 to 9, corresponding to surface coverages from 0 to 1ML. The global optimization method applied in this work has not only accelerated the manual traversal by setting up natural selection based on system energy, but also included all possible surface configurations with multiple adsorbates, greatly enhancing the authenticity of as-organized surface phase diagrams. The detail of workflow of genetic-algorithm-based surface screening applied in this work could be found in Scheme S1 (Supporting Information). The surface structures with lowest energies are displayed in Figures S2–S10 (Supporting Information).

Results and Discussion

The obtained surface phase diagrams are shown in Figure 1. It is obvious that within the wide range of studied CO pressures, there are five separate surface configurations (Figure 1 c–g), with increasing degree of cobalt segregation and consequent increasing CO surface coverage. Under UHV conditions ($< 10^{-7}$ Pa), the CoCu surface only exposes Cu atoms. Under typical CO/CO_2 hydrogenation reaction conditions,[1a] three surface phases might exist, (4/9ML Co, 4/9ML CO), (5/9ML Co, 5/9ML CO) and (1ML Co, 7/9ML CO). We define the former two as moderately segregated and the third as highly segregated, due to the segregation of a complete overlayer of cobalt to the surface. Without CO, Cu dominates the surface, because Cu has lower surface energy than Co (Cu 1.934 J m^{-2} versus Co 2.709 J m^{-2}). The adsorption of CO could drive reverse segregation of Co towards surface, which results from the compensation of enhanced adsorption strength of CO on Co for the increase in surface energy. This phenomenon has been thoroughly studied in our previous work.[9] As the temperature increases from 473 K to 723 K, the regions of (0ML Co, 0ML CO), (4/9ML Co, 4/9ML CO) and (1ML Co, 7/9ML CO) are enlarged, while the regions of (1/9ML Co, 2/9ML CO) and (5/9ML Co, 5/9ML CO) shrink (Figure 1 a,b). We discovered that there are loosely binding CO molecules on (1/9ML Co, 2/9ML CO) and (5/9ML Co, 5/9ML CO), sharing one Co atom or adsorbing on the Co/Cu boundary, destabilizing the surface at higher temperature. The segregation degree of Co not only changes the surface CO coverage but also the molecular adsorption configurations. The higher temperature undermines the thermal stability of surface configuration with loosely dangling, and thus narrows the existing interval of (1/9ML Co, 2/9ML CO) and (5/9ML Co, 5/9ML CO).

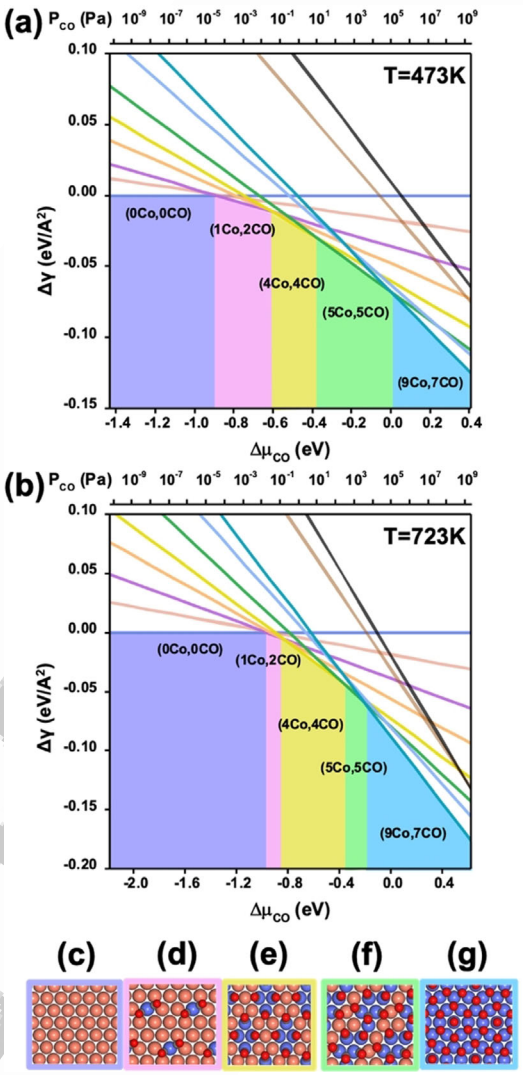

Figure 1. DFT-calculated thermodynamic surface phase diagram of *n*CO adsorbed 3×3 CoCu(111) at a) 473 K and b) 723 K. The diagrams present the Gibbs surface energy $\Delta\gamma$ (eV/A^2) as a function of CO chemical potential $\Delta\mu_{CO}$ (eV) or CO pressure (Pa). And the five screened-out regions are the surfaces of c) (0ML Co, 0ML CO), d) (1/9ML Co, 2/9ML CO), e) (4/9ML Co, 4/9ML CO), f) (5/9ML Co, 5/9ML CO) and g) (1ML Co, 7/9ML CO). For each surface CO coverage, only the surface configuration with the lowest surface energy is shown in the phase diagram, with the other surfaces displayed in the Supporting Information. Atom key: copper (brown), cobalt (blue), carbon (gray), oxygen (red).

Interestingly, the segregated Co tends to form islands rather than be scattered. This phenomenon has been reported before, where Co clusters form on CoCu(110) in dynamic equilibrium with CO atmosphere.[7a] As suggested by Integrated Crystal Orbital Hamilton Population (ICOHP) calculations shown in Figure S11, the Co-Co bonding is far more stable than Cu-Cu and Co-Cu bonding over CoCu(111) surface models, promoting the island formation of Co atoms over CoCu alloy surfaces. With much stronger adsorption strength on cobalt than that on copper, CO prefers bonding on Co ensembles, leading to a relatively CO-free copper surface. This result agrees well with the idea that the low

Dateiname: F109027e
Pfad: l:/daten/verlage/vch/ach/hefte/pool/
Status Neusatz
Datum: 47 KW., 19. November 2021 (Freitag)
Pagina: 3
Seite: 2 te von 7
Umfang (Seiten): 7
Zeit: 10:18:51 Uhr

coverage of reaction species on copper provides space for significant H_2 dissociative chemisorption, with the *CO and *H grouping on different sites over CoCu alloys.[11] It has also been confirmed that the spillover of *H from copper sites to the Co/Cu boundary sustains the hydrogenation reactions.[12] These evidences indicate the hydrogenation steps prefer to proceed at the Co/Cu boundary.

The surface phase diagrams in Figure 1 encompass the dual roles of surface segregation and coverage effect of key adsorbed species, taking one step closer to the realistic modeling of active sites over alloy surfaces. It is also inspiring that the surface segregation of Co or Cu could be well-tuned with different external conditions, e.g., CO partial pressure, based on the proposed surface phase diagram. Next, we calculated the CO_2 hydrogenation reaction networks over the surface models with the highest thermodynamic stability in different CO pressure regions. Note that considering the existence of H_2O and other potential oxidizers in CO/CO_2 hydrogenation process, the alloy surface could be partially oxidized according to previous reports.[3b,7c] Thus, the models applied here only encompass surface segregation and consequent coverage effect over CoCu alloy surfaces, which could describe the active surfaces at the beginning of the catalytic reactions. And the surface phase diagram could qualitatively capture the surface segregation trend of CoCu alloy under different CO partial pressures, though the models are not necessarily identical to exact active surfaces in experiments.

Considering the same pathway applied on CoCu(111) and other surfaces before, and recent experiments on metal catalysts for CO_2 hydrogenation[13] we mainly studied the conversion of CO_2 to CO and further hydrogenation of CO to major products, i.e., CH_4, CH_3OH and C_2H_5OH.[14] According to the supplementary calculation shown in Figure S12, the CO_2 activation is prohibitive on (1ML Co, 7/9ML CO), because gaseous CO_2 is not able to adsorb on the surface with dense arrays of co-adsorbed *CO. Hence, we did not consider the further reaction on this surface (further detailed calculations are presented in the Supporting Information. The transition states of direct C–O breaking of CO_2 are similar on low- and moderate-coverage model surfaces, which have no impact on the selectivity (Figure S13). Here, we mainly focused on the selectivity-determining steps starting from adsorbed *CO.

In CO hydrogenation part, while CH_4 requires C–O bond scission, CH_3OH usually conserves C–O bond in CO_2 or CO, thus the C–O scission step should compete with hydrogenation process to alter selectivity between CH_4 and CH_3OH, e.g., for *CHO, *CH_2O, *CH_2OH, or *CH_3OH.[14] Furthermore, high alcohol production is supposed to happen if C–C coupling and C–O bond scission are both ensured in thermal catalysis.[15] Consequently, selectivity towards higher alcohol should be heavily dependent on the competition of hydrogenation with both C–O bond scission and C–C coupling. The diagram of energy barriers is depicted in Figure 2, from adsorbed *CO to the three major products.

The first observation is that the direct scission of *CO has high energy barriers (>2 eV) on all surfaces considered herein, making it impossible to break the C–O bond without H assistance, in line with calculations on other close-packed transition metal surfaces.[16] The hydrogenation of *CO favors the *CHO rather than *COH intermediate on all surfaces. We rationalize this preference as *CO adsorbs on the surface via the C atom, thus the addition of *H to the O atom in *CO requires *H to migrate from its stable adsorption site to a very unstable state away from the surface, whereas the addition of *H to C is more straightforward. Interestingly, the magnitude of the differences in barrier heights is strongly surface dependent, being only 0.42 eV on (5/9ML Co, 5/9ML CO) compared to 1.26 eV on (1/9ML Co, 2/9ML CO). The narrowed barrier gap is possibly because some *CO is forced to adsorb at a tilted configuration at higher coverages,

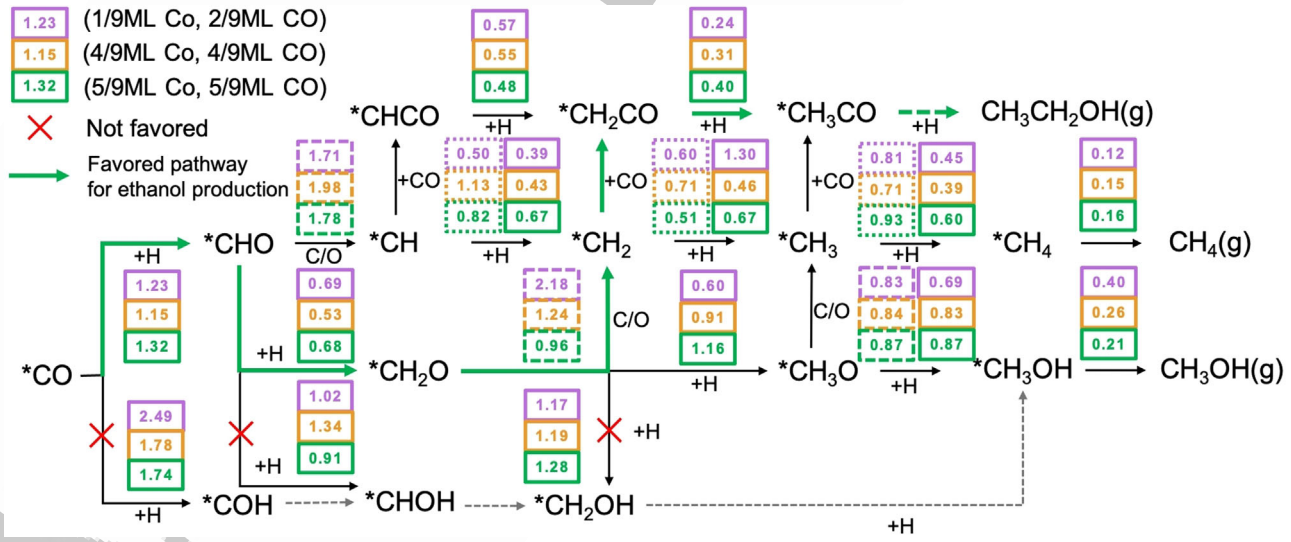

Figure 2. DFT-calculated reaction networks of *CO hydrogenation towards methanol, methane and ethanol. Barriers of hydrogenation are in boxes with a solid line, barriers of C–O scission are in boxes with a long dashed line, and barriers of CO insertion are in boxes with a short dashed line. All values are in eV. The barrier values; (1/9ML Co, 2/9ML CO; purple), (4/9ML Co, 4/9ML CO; orange) and (5/9ML Co, 5/9ML CO; green). The most favored pathway towards ethanol is highlighted with green arrows.

narrowing the hydrogenating distance between surface *H and *O in *CO (Figures S15 and S16).

The most impressive crossroad lies at the bifurcation of $*CH_2O$ (Figure 3a). Reaction barriers of C–O bond scission of $*CH_2O$ dramatically decrease from 2.18 (1/9ML Co, 2/9ML CO) to 0.96 eV (5/9ML Co, 5/9ML CO), even lower than the further hydrogenation to $*CH_3O$ (1.16 eV) or $*CH_2OH$ (1.28 eV) (Figure 3b). Because $*CH_2O$ bonds to surface much weaker than *CO, as for (1/9ML Co, 2/9ML CO) in Figure 3c, the $*CH_2O$ is mainly adsorbed at the copper surface, where the binding strength of transition state (TS) $[*CH_2{-}*OH]^+$ is relatively lower than the cobalt surface areas, giving rise to an extremely high barrier to break the C–O bond. In contrast, on moderate Co-segregated surfaces, $[*CH_2{-}*OH]^+$ could co-adsorb on the Co/Cu boundary, highlighted in yellow rings in Figure 3, and thus be energetically stabilized, which lowers their C–O bond scission barriers.

As for the competing hydrogenation step $*CH_2O + *H = *CH_3O$ in Figure 3d, the TS is a co-adsorption configuration of $[*CH_2O{-}*H]^+$. While the adsorption of $*CH_2O$ on copper domain of (1/9ML Co, 2/9ML CO) is nearly undisturbed by the only *CO, the lateral compelling effect of co-adsorbed *CO on Co ensembles is much more severe on moderate Co segregated surfaces. The weakly-adsorbed $*CH_2O$ is pushed to the rim of the Co/Cu boundary with increasing steric hindrance to accept another *H. The transition states of $*CH_2O + *H = *CH_2OH$ are all close to the configuration of final states, i.e., weakly adsorbed $*CH_2OH$ over the three surfaces, averaging out the effects from almost constant. The inverse changing pattern of barriers between C–O bond scission and further hydrogenation of $*CH_2O$ promotes the formation of $*CH_2$ on moderate segregated surfaces. Moreover, like CO_2, CH_2O is also gas-phase chemically stable molecule under CO_2 hydrogenation conditions. The differential charge density shown in Figure S21 shows that the Cu atom weakly binding CH_2O has little charge redistribution, while the Co atom binding CH_2O strongly has a much larger electron loss, indicating more electrons are transferred to $*CH_2O$ on Co sites. This result agrees with the results of Bader charge analysis that $*CH_2O$ species is negatively charged ($0.23\,e^-$) on Co ensemble, while almost neutrally charged ($0.01\,e^-$) on Cu sites. And the calculated adsorption energy of $*CH_2O$ on Co sites is ca. 0.27 eV stronger than the physical adsorption on Cu site, indicating the stronger interaction between CH_2O and surface Co ensembles. Surprisingly, after $*CH_2O$ is split to $*CH_2$, the methanation process is energetically less likely than CO insertion on (5/9ML Co, 5/9ML CO), resulting in a more kinetically favored formation of $*CH_2CO$, a key precursor to ethanol production (Figures S19 and S20). *CO. Thus, the barriers of $*CH_2OH$ formation are almost constant. Consequently, one would expect a promoted ethanol selectivity on moderate Co segregated surfaces, where the Cu domains confine the size of Co islands to avoid the over-binding of *CO. The similar phenomenon has also been reported on CoGa alloys for ethanol production from syngas, where Ga plays a diluting role similar to Cu here.[15b]

Inspired by the surface phase diagram depicted in Figure 1, we synthesized a series of CoCu alloys via a refined two-step procedure based on the previous oxalate route shown in Figure 4a.[7c] The detailed synthesis procedures can be found under "Catalyst Preparation" in the Supporting Information. The surface-sensitive X-ray photoelectron spectroscopy (XPS) was used to characterize the surface elemental composition of CoCu alloy samples pretreated under different CO partial pressures.

A pseudo core–shell CoCu alloy structure mainly exposing CoCu(111) facets (Figure 4b) of S-1 % CO catalyst could be observed by aberration-corrected Scanning Transmission Electron Microscopy in Figure 4c, indicating the strong surface elemental segregation during segregation-inducing step. The EDS line profile of the same sample in Figure S25 also shows a Co-rich surface and Cu-rich core structure after CO-inducing procedure. In Figure 4d, the surface Co/Cu ratio of fresh catalysts increases from trace amount to 2.23 with the increasing CO partial pressures. The S-1 % CO (S-: catalyst sample) corresponds to approximately 1 kPa CO partial pressure in segregation-inducing step, leading to a 50 % Co-segregated CoCu surface structure, in good agreement with the moderate segregation region (5/9ML Co, 5/9ML CO) in Figure 1b. In parallel, the CO adsorption peak of S-10 % CO ($1972\,cm^{-1}$) shifts to lower wavenumbers than that of S-1 % CO ($1981\,cm^{-1}$) and S-0.1 % CO ($2002\,cm^{-1}$) measured by in situ Diffuse Reflectance Infrared Fourier Transform Spectroscopy (DRIFTS) in (Figure S28), also shows the enhancement of adsorption strength of CO as the CO partial pressure increases during segregation-inducing step. Theoretically, the calculated CO asymmetry stretching frequency also decreased from $2011\,cm^{-1}$, on-top site of Cu atoms for low coverage, to $1954\,cm^{-1}$, on Co atoms in (5/9ML Co, 5/9ML CO) model.

The experimental evidence above confirms the feasibility of tuning surface composition on

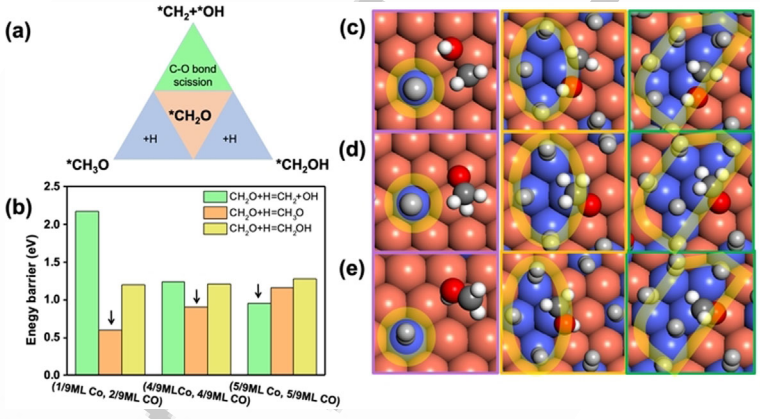

Figure 3. The competition of C–O bond scission in $*CH_2O$ and $*CH_2O$ further hydrogenation reactions. a) Further reactions for key intermediate $*CH_2O$. b) The energy profile for C–O bond scission and further hydrogenation of $*CH_2O$ on three surfaces. c) The transition states of C–O bond scission of $*CH_2O$ on three surfaces. d,e) Further hydrogenation to $*CH_3O$ or $*CH_2OH$. Key: Co/Cu boundary sites (half-transparent yellow rings), spectator *CO (gray).

Dateiname: F109027e
Pfad: l:/daten/verlage/vch/ach/hefte/pool/
Status Neusatz
Datum: 47 KW., 19. November 2021 (Freitag)
Pagina: 5
Seite: 4 te von 7
Umfang (Seiten): 7
Zeit: 10:18:52 Uhr

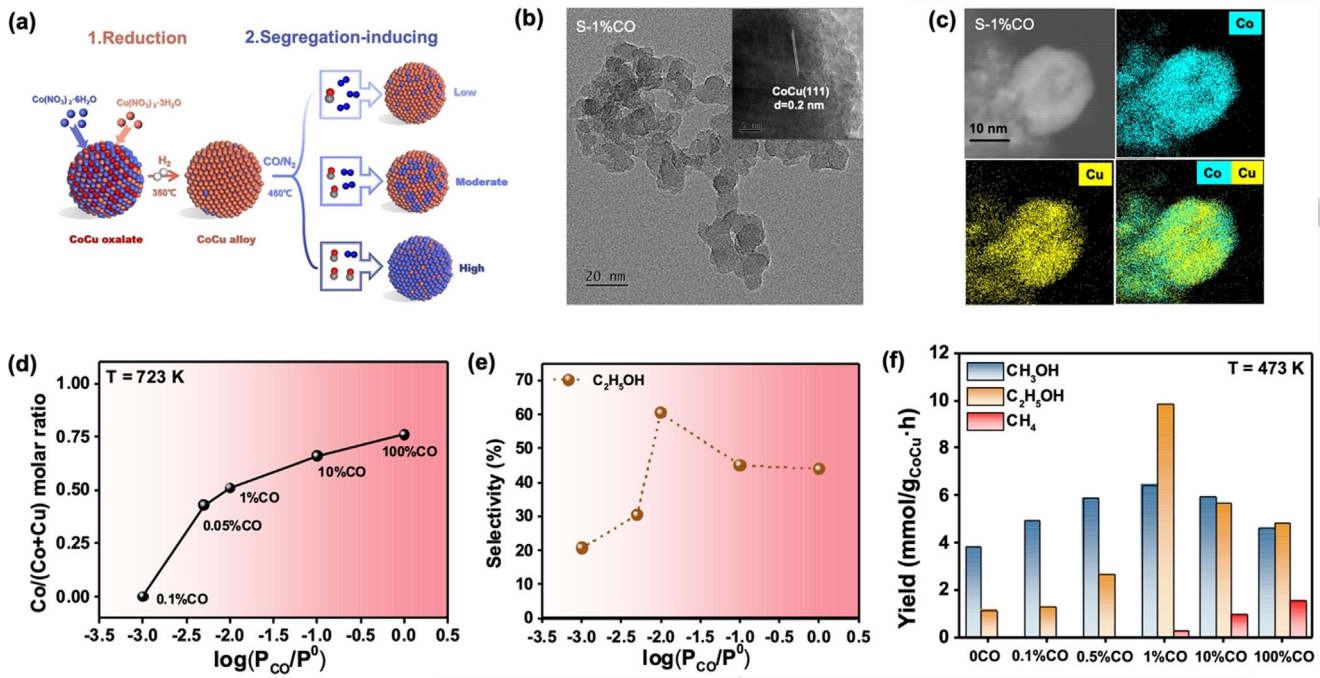

Figure 4. Experimental results of CoCu catalysts in CO_2 hydrogenation reactions: $H_2/CO_2 = 3:1$, $P_{total} = 4$ MPa, and $T = 473$ K. a) The synthesis methodology for CoCu alloys with different Co surface segregation degree: low, moderate and high. b) High-resolution TEM (HRTEM) images. c) Aberration corrected scanning TEM high-angle annular dark-field images and element distribution of as-synthesized S-1%CO. d) XPS results for the CoCu surface Co/Cu ratios after prereduction procedures, $P^0 = 0.1$ MPa. e) The relationship between selectivity of ethanol and CO pressure. f) The relationship between yield of ethanol and CO pressure. The values in front of CO in the X axis represent the ratio of $CO/(N_2 + CO)$ in prereduction procedures.

account of the prediction of surface phase diagram. However, we could also see the limitation of the prediction. As the CO pressure approaches 0.1 MPa, the actual CoCu surface is not covered by pure cobalt, but only ca. 75% of Co segregate to the surface. Also, the surface phase diagram overestimates the effect of CO to induce Co segregation in the low-pressure regime. Nevertheless, the thermodynamic surface diagram could qualitatively predict the trend of surface segregation, offering important theoretical guidance for catalyst optimization, especially for surfaces sensitive to gas conditions.

Furthermore, the CoCu alloy samples were tested in CO_2 hydrogenation at the same conditions: $H_2/CO_2 = 3:1$, $P_{total} = 4$ MPa, and $T = 473$ K. Impressively, a selectivity volcano to ethanol production is obtained in Figure 4e, in agreement with the calculations of CO_2 hydrogenation networks above. At S-1%CO, both the yield and selectivity reach the maximum, with a 61% selectivity towards ethanol. Continuing to increase CO pressure, the selectivity reduces by 18% on S-10%CO and by 20% on S-100%CO. Similarly, a volcano-like plot of ethanol yield can also be found in Figure 4f. Temperature-programmed surface reaction (TPSR) analysis was used to evaluate the intrinsic activity of the catalysts for C–O bond cleavage. In Figure S27, C–O cleavage and CH_4 formation starts at ca. 200°C on S-10%CO and 250°C on S-1%CO, while the MS signal of CH_4 was extremely weak for S-0.1%CO. This result supports that S-1%CO shows moderate capacity for C–O cleavage due to a moderately CO-induced CoCu surface. The weak ability to activate C–O on Cu-rich S-0.1%CO inhibits the generation of ethanol and thus methanol is the major product. In contrast, Co-rich S-10%CO starts methane production, due to facile C–O cleavage on Co ensembles.

By modulating the CoCu surface to a moderate Co segregation state at the beginning of the reaction, we were able to promote ethanol production in CO_2 hydrogenation reactions, reaching over 60% selectivity towards ethanol, at the same time completely avoiding methane production. Despite in situ surface oxidation and restructuring might occur during hydrogenation process, the theory still holds based on surface models from surface phase diagram, at least for the fresh catalysts. Considering the same overall Co/Cu elemental ratio in different raw catalysts and the same hydrogenation reaction conditions, the prereduction procedure that modifies the surface distribution of the alloy should play a crucial role in the volcano-like catalytic performance in CO_2 hydrogenation reactions. The accumulative yield and selectivity results in Figure 4f after 12 h of reaction indicates the CoCu active surfaces are intrinsically different after being pre-reduced in different gas conditions. The results shown above display qualitative prediction ability of the workflow of theory-based catalyst optimization exemplified in this article (Scheme S2). And the workflow is believed to be transferable to other similar systems, e.g., NiAu[8a] and CuNi[8b] alloy in CO_2 hydrogenation, AgCu[18]■■Please cite ref. [17] in the appropriate position■■ alloy in epoxidation reactions, PtSn[19] and CoPd[20] nanocatalysts in CO oxidation, etc.

Conclusion

In brief, based on a theoretical surface phase diagram from global searching, we have demonstrated that the segregation of Co atoms over the CoCu surface accompanies an increased CO coverage, changing catalytic performance via both surface segregation and coverage effect. The promoted C–O scission of $*CH_2O$ and competent C–C coupling computationally predicts a high ethanol selectivity over the CoCu surface with moderate Co segregation. Applying a two-step reduction-induction procedure, we successfully obtained $>60\%$ ethanol selectivity over the moderately CO-induced CoCu catalyst, despite possible surface oxidation and restructuring during reactions. These exciting discoveries strongly underpin the vision of a theory-based optimization workflow for excellent industrialized catalysts, especially for alloy systems with segregation tendencies in certain conditions.

Acknowledgements

S.L., C.Y., Z.Z., J.G. acknowledge the National Key Research and Development Program of China (2016YFB0600901), the National Science Foundation of China (21525626 and 21761132023), and the Program of Introducing Talents of Discipline to Universities (No.BP0618007) for financial support. F.S. gratefully acknowledges financial support from Deutsche Forschungsgemeinschaft (STU 703/1-1), and by the Helmholtz Association.

Conflict of Interest

The authors declare no conflict of interest.

Keywords: catalyst optimization · CO_2 · CoCu alloy · ethanol production · surface segregation

[1] a) H. T. Luk, C. Mondelli, D. C. Ferre, J. A. Stewart, J. Perez-Ramirez, *Chem. Soc. Rev.* **2017**, *46*, 1358 – 1426; b) Z. Shi, H. Yang, P. Gao, X. Li, L. Zhong, H. Wang, H. Liu, W. Wei, Y. Sun, *Catal. Today* **2018**, *311*, 65 – 73.

[2] M. Behrens, F. Studt, I. Kasatkin, S. Kuhl, M. Havecker, F. Abild-Pedersen, S. Zander, F. Girgsdies, P. Kurr, B. L. Kniep, M. Tovar, R. W. Fischer, J. K. Norskov, R. Schlögl, *Science* **2012**, *336*, 893 – 897.

[3] a) Y. Xiang, N. Kruse, *J. Energy Chem.* **2016**, *25*, 895 – 906; b) J. Su, Z. Zhang, D. Fu, D. Liu, X.-C. Xu, B. Shi, X. Wang, R. Si, Z. Jiang, J. Xu, Y.-F. Han, *J. Catal.* **2016**, *336*, 94 – 106; c) Y. Xiang, V. Chitry, P. Liddicoat, P. Felfer, J. Cairney, S. Ringer, N. Kruse, *J. Am. Chem. Soc.* **2013**, *135*, 7114 – 7117.

[4] a) A. Cao, J. Schumann, T. Wang, L. Zhang, J. Xiao, P. Bothra, Y. Liu, F. Abild-Pedersen, J. K. Nørskov, *ACS Catal.* **2018**, *8*, 10148 – 10155; b) J. Schumann, A. J. Medford, J. S. Yoo, Z.-J. Zhao, P. Bothra, A. Cao, F. Studt, F. Abild-Pedersen, J. K. Nørskov, *ACS Catal.* **2018**, *8*, 3447 – 3453; c) A. J. Medford, A. C. Lausche, F. Abild-Pedersen, B. Temel, N. C. Schjødt, J. K. Nørskov, F. Studt, *Top. Catal.* **2014**, *57*, 135 – 142.

[5] S. Carenco, A. Tuxen, M. Chintapalli, E. Pach, C. Escudero, T. D. Ewers, P. Jiang, F. Borondics, G. Thornton, A. P. Alivisatos, H. Bluhm, J. Guo, M. Salmeron, *J. Phys. Chem. C* **2013**, *117*, 6259 – 6266.

[6] G. Collinge, N. Kruse, J.-S. McEwen, *J. Catal.* **2018**, *368*, 31 – 37.

[7] a) B. Eren, D. Torres, O. Karslioglu, Z. Liu, C. H. Wu, D. Stacchiola, H. Bluhm, G. A. Somorjai, M. Salmeron, *J. Am. Chem. Soc.* **2018**, *140*, 6575 – 6581; b) G. Collinge, N. Kruse, J.-S. McEwen, *J. Phys. Chem. C* **2017**, *121*, 2181 – 2191; c) Y. Xiang, R. Barbosa, N. Kruse, *ACS Catal.* **2014**, *4*, 2792 – 2800.

[8] a) X. Zhang, S. Han, B. Zhu, G. Zhang, X. Li, Y. Gao, Z. Wu, B. Yang, Y. Liu, W. Baaziz, O. Ersen, M. Gu, J. T. Miller, W. Liu, *Nat. Catal.* **2020**, *3*, 411 – 417; b) I. Zegkinoglou, L. Pielsticker, Z.-K. Han, N. J. Divins, D. Kordus, Y.-T. Chen, C. Escudero, V. Perez-Dieste, B. Zhu, Y. Gao, B. Roldan Cuenya, *J. Phys. Chem. C* **2019**, *123*, 8421 – 8428; c) M. A. van Spronsen, K. Daunmu, C. R. O'Connor, T. Egle, H. Kersell, J. Oliver-Meseguer, M. B. Salmeron, R. J. Madix, P. Sautet, C. M. Friend, *J. Phys. Chem. C* **2019**, *123*, 8312 – 8323.

[9] S. Liu, Z.-J. Zhao, C. Yang, S. Zha, K. M. Neyman, F. Studt, J. Gong, *ACS Catal.* **2019**, *9*, 5011 – 5018.

[10] a) F. C. Chuang, C. V. Ciobanu, V. B. Shenoy, C. Z. Wang, K. M. Ho, *Surf. Sci.* **2004**, *573*, L375 – L381; b) S. Liu, J. Zong, Z.-J. Zhao, J. Gong, *Green Chem. Eng.* **2020**, *1*, 56 – 62.

[11] E. A. Lewis, D. Le, A. D. Jewell, C. J. Murphy, T. S. Rahman, E. C. Sykes, *Chem. Commun.* **2014**, *50*, 6537 – 6539.

[12] E. A. Lewis, M. D. Marcinkowski, C. J. Murphy, M. L. Liriano, E. C. Sykes, *J. Phys. Chem. Lett.* **2014**, *5*, 3380 – 3385.

[13] N. Yang, A. J. Medford, X. Liu, F. Studt, T. Bligaard, S. F. Bent, J. K. Norskov, *J. Am. Chem. Soc.* **2016**, *138*, 3705 – 3714.

[14] a) F. Romero-Sarria, L. F. Bobadilla, E. M. Jiménez Barrera, J. A. Odriozola, *Appl. Catal. B* **2020**, *272*, 119032; b) C. Yang, S. Liu, Y. Wang, J. Song, G. Wang, S. Wang, Z. J. Zhao, R. Mu, J. Gong, *Angew. Chem. Int. Ed.* **2019**, *58*, 11242 – 11247; *Angew. Chem.* **2019**, *131*, 11364 – 11369; c) L. Liu, F. Fan, Z. Jiang, X. Gao, J. Wei, T. Fang, *J. Phys. Chem. C* **2017**, *121*, 26287 – 26299.

[15] a) L. Wang, L. Wang, J. Zhang, X. Liu, H. Wang, W. Zhang, Q. Yang, J. Ma, X. Dong, S. J. Yoo, J. G. Kim, X. Meng, F. S. Xiao, *Angew. Chem. Int. Ed.* **2018**, *57*, 6104 – 6108; *Angew. Chem.* **2018**, *130*, 6212 – 6216; b) Z. An, X. Ning, J. He, *J. Catal.* **2017**, *356*, 157 – 164.

[16] a) S. Lin, J. Ma, X. Ye, D. Xie, H. Guo, *J. Phys. Chem. C* **2013**, *117*, 14667 – 14676; b) C. Chen, Q. Wang, G. Wang, B. Hou, L. Jia, D. Li, *J. Phys. Chem. C* **2016**, *120*, 9132 – 9147.

[17] D. Mei, R. Rousseau, S. M. Kathmann, V.-A. Glezakou, M. H. Engelhard, W. Jiang, C. Wang, M. A. Gerber, J. F. White, D. J. Stevens, *J. Catal.* **2010**, *271*, 325 – 342.

[18] L. A. Cramer, Y. Liu, P. Deshlahra, E. C. H. Sykes, *J. Phys. Chem. Lett.* **2020**, *11*, 5844 – 5848.

[19] M. Vandichel, A. Moscu, H. Grönbeck, *ACS Catal.* **2017**, *7*, 7431 – 7441.

[20] C. H. Wu, C. Liu, D. Su, H. L. Xin, H.-T. Fang, B. Eren, S. Zhang, C. B. Murray, M. B. Salmeron, *Nat. Catal.* **2019**, *2*, 78 – 85.

Manuscript received: July 7, 2021
Revised manuscript received: September 29, 2021
Accepted manuscript online: October 22, 2021
Version of record online: ■■ ■■, ■■■■

Research Articles

CO_2 Hydrogenation

S. Liu, C. Yang, S. Zha, D. Sharapa, F. Studt, Z. Zhao,* J. Gong ——— ■■■■–■■■■

Moderate Surface Segregation Promotes Selective Ethanol Production in CO_2 Hydrogenation Reaction over CoCu Catalysts

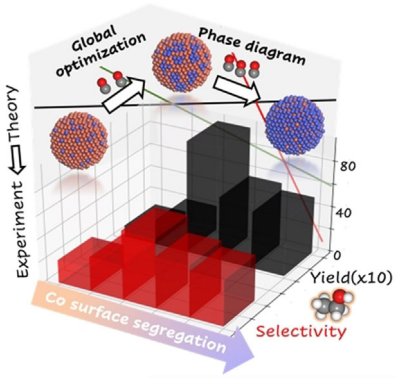

A method is described for theory-based catalyst optimization of CoCu alloys in CO_2 hydrogenation. Moderate Co surface segregation, boosted ethanol production, and suppressed methane generation suggest that theory-guided catalyst optimization could be beneficial in similar alloy systems.

CO_2 Hydrogenation

S. Liu, C. Yang, S. Zha, D. Sharapa, F. Studt, Z. Zhao,* J. Gong ——— ■■■■–■■■■

Moderate Surface Segregation Promotes Selective Ethanol Production in CO_2 Hydrogenation Reaction over CoCu Catalysts

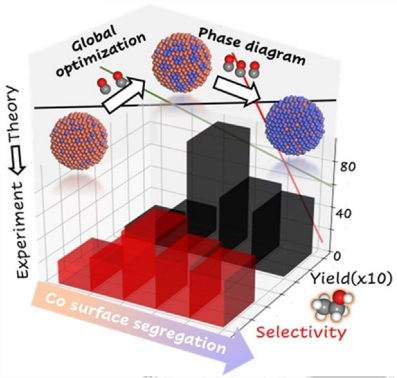

A method is described for theory-based catalyst optimization of CoCu alloys in CO_2 hydrogenation. Moderate Co surface segregation, boosted ethanol production, and suppressed methane generation suggest that theory-guided catalyst optimization could be beneficial in similar alloy systems.

SPACE RESERVED FOR IMAGE AND LINK

Share your work on social media! *Angewandte Chemie* has added Twitter as a means to promote your article. Twitter is an online microblogging service that enables its users to send and read short messages and media, known as tweets. Please check the pre-written tweet in the galley proofs for accuracy. If you, your team, or institution have a Twitter account, please include its handle @username. Please use hashtags only for the most important keywords, such as #catalysis, #nanoparticles, or #proteindesign. The ToC picture and a link to your article will be added automatically, so the **tweet text must not exceed 250 characters**. This tweet will be posted on the journal's Twitter account (follow us @angew_chem) upon publication of your article in its final (possibly unpaginated) form. We recommend you to re-tweet it to alert more researchers about your publication, or to point it out to your institution's social media team.

Please check that the ORCID identifiers listed below are correct. We encourage all authors to provide an ORCID identifier for each coauthor. ORCID is a registry that provides researchers with a unique digital identifier. Some funding agencies recommend or even require the inclusion of ORCID IDs in all published articles, and authors should consult their funding agency guidelines for details. Registration is easy and free; for further information, see http://orcid.org/.

Sihang Liu
Dr. Chengsheng Yang
Shenjun Zha
Dr. Dmitry Sharapa
Prof. Dr. Felix Studt
Prof. Dr. Zhi-Jian Zhao http://orcid.org/0000-0002-8856-5078
Prof. Dr. Jinlong Gong

These are not the final page numbers!

Dateiname: F109027e
Pfad: I:/daten/verlage/vch/ach/hefte/pool/
Status Neusatz
Datum: 47 KW., 19. November 2021 (Freitag)
Pagina: 8
Seite: 7 te von 7
Umfang (Seiten): 7
Zeit: 10:18:54 Uhr